**PASJ:** Publ. Astron. Soc. Japan **59**, 799–809, 2007 August 25


# A Pole-on Bipolar Outflow from the AGB Star WX Piscium

Noritomo INOMATA
*Graduate School of Science and Engineering, Kagoshima University, 1-21-35 Korimoto, Kagoshima, Kagoshima 890-0065*
and
Hiroshi IMAI and Toshihiro OMODAKA
*Department of Physics, Faculty of Science, Kagoshima University, 1-21-35 Korimoto, Kagoshima, Kagoshima 890-0065*
*hiroimai@sci.kagoshima-u.ac.jp, omodaka@sci.kagoshima-u.ac.jp*

(Received 2007 January 17; accepted 2007 April 16)

**Abstract**

We report on $H_2O$ masers around the asymptotic giant branch (AGB) star WX Piscium (WX Psc = IRC +10011), observed with the Japanese VLBI Network (JVN) at three epochs during a span of 2 months. The $H_2O$ maser spectrum of WX Psc consists of double peaks with a separation of $\sim$ 30 km s$^{-1}$ centered at the systemic velocity of the star. The maser features are found to split roughly in two concentrations separated by about 60 mas from north to south. The northern concentration involves both blueshifted and redshifted components from both of the double peaks, suggesting that it is near the star driving the outflow. The maser spatiokinematics is well approximated by a radial expansion of a thick shell, except for the blueshifted features in the southern concentration. The spatiokinematics is compared with a fan-shaped morphology found in near-infrared emission, suggesting the existence of a bipolar outflow. Two different models are proposed for explaining the observed maser proper motions: one is a biconically expanding flow with a large opening angle ($2\theta_{\rm cone}$ =70°–120°); the other is a collimated outflow with precession. The complicated spatiokinematics of the $H_2O$ maser features indicates that the star is currently in the process of launching a bipolar outflow in the final stage of the AGB phase, shaping a planetary nebula in the next stage.

**Key words:** masers — stars: AGB and post-AGB — stars: individual(WX Piscium) — stars: winds, outflows

## 1. Introduction

The question of how a planetary nebula (PN) is shaped at the final stage of stellar evolution is one of the most interesting issues in astronomy. Planetary nebula shaping from a spherically symmetric circumstellar envelope has been considered to occur by interactions of a slowly expanding cool wind with a fast and hot wind. Both winds are formed by the same evolved star, but the former is formed in the asymptotic giant branch (AGB) phase, while the latter is launched later in the post-AGB phase (Kwok et al. 1978). However, a spherical wind can produce only a spherically symmetric PN. Nowadays there is evidence to show that a large fraction of planetary nebulae are more or less asymmetric. It is expected that shaping an asymmetric PN is due to the interaction of a fast, collimated flow with a slowly expanding AGB wind. The collimated flow is assumed to be ignited at the end of the AGB phase or the beginning of the post-AGB phase (e.g., Imai et al. 2002). Based on the universal connection between bipolar flows and rotating strong magnetic fields (AGNs, micro- and nano-quasars, protostars, and pulsars), a process that is similar to the magneto-centrifugal mechanism is expected to generate such collimated flows in AGB/post-AGB stars (e.g., Blackman et al. 2001; Vlemmings et al. 2006).

Collimated bipolar flows are seen as high-velocity components in atomic-emission lines in post-AGB stars when the AGB envelopes change into pre-PNe, or have already started their photoionization. Such flows are also found in spectra of molecular-emission lines (e.g., $H_2O$ maser) in AGB stars as components with velocities much larger than a typical expansion velocity of a circumstellar envelope traced by CO and OH lines (20–30 km s$^{-1}$, e.g., te Lintel Hekkert et al. 1989). There have been a small number ($\sim$10) of candidates for such high-velocity sources; some of them have been mapped in $H_2O$ maser emission with high angular resolution, e.g., IRAS 16342−3814, OH 12.8−0.9, W43A, and IRAS 19134+2131 (Imai et al. 2002, 2004, 2005; Morris et al. 2003; Boboltz & Marvel 2005; Vlemmings et al. 2006). They have flow velocities higher than 30 km s$^{-1}$, some of them over 100 km s$^{-1}$. It is interesting to investigate circumstellar envelopes at an earlier phase, in which a bipolar flow may have just been launched with a lower velocity. Because such very young bipolar flows are not well developed and are apparently physically compact, observations with high resolution ($\lesssim$10 mas) are essential.

WX Piscium (WX Psc = IRC +10011, CIT 3, IRAS 01037+1219) is an oxygen-rich long-period variable with a mean infrared variability period of 660 d (Le Bertre 1993) and is one of the extremely reddened infrared AGB stars. This star has a spectral type of M9–10 (Dyck et al. 1974; Lockwood 1985) and is surrounded by a thick dust shell; its mass-loss rate is estimated to be $\sim 10^{-5}\ M_\odot {\rm yr}^{-1}$. SiO (e.g., Blair & Dickinson 1977; Desmurs et al. 2000), $H_2O$ (e.g., Dickinson et al. 1978; Comoretto et al. 1990), and OH (e.g., Wilson et al. 1970; Olnon et al. 1980) maser lines have been detected. OH maser and CO line observations provide an estimated expansion velocity of the circumstellar shell of 20 km s$^{-1}$ (Baud 1981; Loup et al. 1993) and a

systemic radial velocity of WX Psc of $V_{\rm LSR}$= 9.7 km s$^{-1}$ (Cernicharo et al. 1997). The distance to WX Psc has been estimated to be in the range of 500–800 pc (e.g., Hyland et al. 1972; Baud 1981; Bowers et al. 1983; van Langevelde et al. 1990; Whitelock et al. 1994). In the present paper, we adopt a distance of 650 pc.

Hofmann et al. (2001, hereafter H01) carried out a near-infrared bispectrum speckle-interferometric observation of WX Psc in the $J$-, $H$-, and $K'$-bands with angular resolutions of 48, 56, and 73 mas, respectively. The $H$- and $K'$-band images exhibit almost a spherically symmetric structure, while the $J$-band image reveals two components: a compact elliptical core and a fainter fan-shaped structure extended northwestward. Vinković et al. (2004, hereafter V04) performed a two-dimensional radiative transfer calculation to reproduce the images obtained by H01. They assumed bidirectional cones with an $r^{-0.5}$ density profile, which are embedded in a spherically expanding wind with a standard $r^{-2}$ density profile. The bicone model suggests that the fast, bipolar jet sweeps up material in the slower spherical wind and creates an elongated cocoon that produces the observed asymmetry in the NIR image. On the other hand, the SiO masers roughly exhibit a circular ring morphology at 2–3 stellar radii from the central star (e.g., Desmurs et al. 2000; Soria-Ruiz et al. 2004, 2005), a structure often seen in AGB stars (e.g., Diamond et al. 1994; Miyoshi et al. 1994; Greenhill et al. 1995).

In the present paper, we report on three-epoch VLBI observations of $H_2O$ masers associated with WX Psc, designed to elucidate the spatiokinematics of the masers and to find more direct evidence for the existence of a bipolar outflow associated with this star. The $H_2O$ maser spectrum shows clear double-emission peaks separated by $\sim$30 km s$^{-1}$. It is quite unique among $H_2O$ maser spectra found in many Mira-type AGB stars, which often show multiple-velocity components within a smaller velocity range ($\leq$ 20 km s$^{-1}$: Takaba et al. 1994).

## 2. Observations and Data Reduction

VLBI observations using the Japanese VLBI network (JVN) were carried out on 2005 March 24, April 27, and May 28. This network consists of six telescopes in the 22 GHz band: the 45 m telescope at Nobeyama, the 34 m telescope at Kashima, and four 20 m antennas of the VLBI Exploration of Radio Astrometry (VERA) located at Mizusawa, Iriki, Ogasawara, and Ishigakijima (e.g., Imai et al. 2006). The observation durations were 8 hr for the first epoch and 10 hr for the other epochs. However, during the third epoch the Nobeyama telescope joined for only the first 6 hr. The system noise temperatures at the zenith were typically 150–200 K during the first two epochs and 200–250 K during the third. Left-hand circular polarization signals were digitized and recorded using the SONY DIR-1000 recorder at a rate of 128 Mbps with 2 bit quantization. Among the total bandwidth of 32 MHz, one 16 MHz channel was assigned to WX Psc, covering a radial velocity span of 215.7 km s$^{-1}$. Another 16 MHz was used to detect a phase-reference radio source with VERA's dual-beam system; unfortunately, this was not detected, and is therefore not reported in the present paper. The data were correlated with the Mitaka FX correlator with 1024 spectral channels per 16 MHz, yielding frequency and velocity resolutions of 15.6 kHz and 0.21 km s$^{-1}$, respectively.

We applied a standard calibration method for the maser data using the Astronomical Image Processing System (AIPS) of the National Radio Astronomy Observatory (NRAO). For visibility-amplitude calibration, the "template spectrum method" (e.g., Diamond 1989, 1995) was performed to obtain an accurate *relative* time variation in the flux-density scale for each telescope with a time resolution of 1 min. This includes the time variation both in the telescope gain due to beam offset and in the system noise temperature. The absolute flux-density scale, determined from calibrator sources, has a large uncertainty of about 20%. Calibration for clock delay offsets, which introduce erratic phase gradients across velocity channels, was made by using data of the continuum calibrator (ICRF J020450.4+151411). The uncertainties in the estimated offsets were smaller than 5 ns, corresponding to a position drift with a frequency of 6.2 microarcsec per MHz at a baseline length of 1300 km. Because WX Psc is a nearby source, any cross-correlated flux is significantly decreased on the longer baselines. Thus, we only used the baselines between the Nobeyama 45 m, the Kashima 34 m, and the VERA-Mizusawa 20 m telescopes. We selected the velocity channel of $V_{\rm LSR}$ = $-$3.6 km s$^{-1}$ as the phase-reference channel in all of the observing sessions. Very bright maser emission in this channel was used for fringe-fitting and self-calibration procedures, which removed any erratic phase variation with time. The hybrid mapping method, repeating the self-calibration and CLEAN imaging (e.g., Wilkinson 1989), was performed to solve both the complex calibration gains of the telescopes and the source structure. The final solution interval of the complex calibration gains was set to 12 s, which was short enough to compensate for any phase fluctuation due to the Earth's atmosphere, and long enough to obtain signal-to-noise ratios higher than 10. The fringe-fitting and self-calibration solutions were applied to all of the velocity channels to obtain maser image cubes.

We then made CLEAN image cubes for selected fields with maser emission. The field of view of the CLEAN map was 128 mas $\times$ 128 mas. Uniformly weighted visibility data created a synthesized beam of 7.5 mas $\times$ 3.4 mas with a position angle of $-70^\circ$. Such a large synthesized beam was formed by flagging the long-baseline data. The detection limit was about 250 mJy $\mathrm{beam}^{-1}$ at an 8 $\sigma$ noise level in all of the observation sessions. The dynamic range equivalent to a ratio of the peak intensity-to-noise reached 600 : 1 in the best case. The positions of the brightness peaks in the detected maser components were estimated using the AIPS task SAD by assuming a two-dimensional Gaussian brightness distribution. The uncertainty of the estimated position depends on the signal-to-noise ratio of the maser component, whose typical value was 50 microarcsec for an 1 Jy component. At the third epoch, the position uncertainty was larger than those at other epochs, which caused a poorer accuracy of the measured maser proper motions. Table 1 gives a summary of the present VLBI observations and maser images.

## 3. Results

As mentioned above, the $H_2O$ maser emission in WX Psc is significantly spatially resolved. Figure 1 shows the cross-power spectrum obtained from the Nobeyama 45 m–Kashima 34 m baseline. Even for the shortest baseline in the JVN, only ∼15% of the total flux density was detected. The spectrum clearly shows double peaks, the blueshifted ($V_{\rm LSR} = -6$–$0$ km s$^{-1}$) and redshifted ($V_{\rm LSR} = 20$–$24$ km s$^{-1}$) components. The velocity separation of ∼25 km s$^{-1}$ between the double peaks has persisted since previous single-dish observations (Dickinson et al. 1978; Comoretto et al. 1990). The center velocity of the double peaks is $V_{\rm LSR} \simeq 10$ km s$^{-1}$, which is consistent with that obtained by a previous CO observation (Cernicharo et al. 1997). Table 2 shows parameters of all detected maser features. Figure 2 shows the spatial distribution of $H_2O$ maser emission at each epoch. The maser spectrum is similar to that found in the 1612 MHz OH maser emission, indicating the existence of a spherically expanding flow or a bipolar outflow. It is also similar to the $H_2O$ maser emission in the "water fountain" sources (e.g., Imai et al. 2002). However, the blueshifted and redshifted components are distributed differently, and some parts of them overlap. The whole distribution size is 100 mas × 80 mas, corresponding to 65 AU × 52 AU at 650 pc in the RA and Dec directions.

We measured the relative proper motion of each maser feature with respect to the reference feature. Superposing the three-epoch maser maps, we found that the same maser feature at $V_{\rm LSR} = 3.7$ km s$^{-1}$ was detected at all epochs, which we therefore used as a position reference. In order to obtain the proper motion, a least-squares fitting method was used with a weight inversely proportional to the square of the position error for each data point. Figure 3 shows temporal variations, in RA and Dec offsets and in LSR velocity, of the maser features whose proper motions were measured. Table 3 lists the measured proper motions, radial motions, and peak intensities of the maser features. Only 13 maser proper motions out of ∼20 detected features were obtained, indicating that individual maser features turn on and off on a time scale of a few months.

Figure 4 shows the locations and proper motions of the maser features on the sky. The three-dimensional velocity field of $H_2O$ masers marginally exhibits systematic expansion of the circumstellar envelope. Adopting a model-fitting method shown in Imai et al. (2000), which assumes a pure radial expansion with independent expansion velocities of maser features, we estimated the location of the dynamical center of the expanding flow. The center is located on the sky plane at $(X, Y) = (-12, 60)$ [mas] (which is indicated with a plus symbol in figure 4), and moving with a velocity vector of $(V_{\rm Xc}, V_{\rm Yc}) = (-0.6, 5.2)$ [km s$^{-1}$] with respect to the position-reference maser feature.

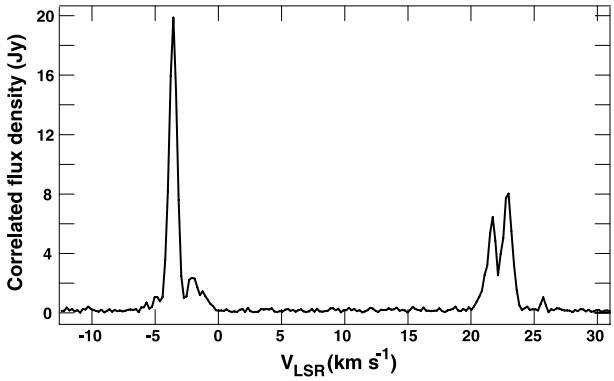


**Fig. 1.** Cross-power spectrum of $H_2O$ masers in WX Psc obtained on the baseline between the NRO 45 m and NICT 34 m telescopes during the first epoch.

To estimate the spatial locations and expansion velocities of individual maser features in the envelope, we adopted an expanding thick-shell model; the shell consists of several thin shells each of which satisfies the equation for the observed radial velocity and projected distance from the star $(V, r)$ as

$$\left(\frac{r}{r_{\rm shell}}\right)^2 + \left(\frac{V - V_{\rm sys}}{V_{\rm exp}}\right)^2 = 1. \quad (1)$$

Here, $r_{\rm shell}$ is the radius of the thin shell, $V_{\rm exp}$ the expansion velocity of the thin shell, and $V_{\rm sys}$ the systemic velocity of WX Psc. Figure 5 shows the projected distance–radial-velocity diagram of the maser spots (velocity components). Typically, a maser feature consists of maser spots having similar radial velocities spanning a 1–2 km s$^{-1}$ width. Note that the maser spot distribution is not continuous in radius, The greater part of maser spots are associated with a few expanding thin shells with discrete radii; such a situation is also found in other $H_2O$ masers in Mira variables (e.g., Bains et al. 2003). They seem to be associated with a thick shell with inner and outer radii of ∼25 mas and ∼40 mas, respectively, and an expansion velocity of ∼10 km s$^{-1}$ with acceleration up to ∼25 km s$^{-1}$. We also found a group of maser spots that are located over 50 mas south of the central star (see figure 4). If we assume that the southern group is also associated with the shell with

**Table 1.** Status of the telescopes, data reduction, and resulting performances in the individual epochs of the JVN observations.

| Observation code | Epoch in the year 2005 | Duration (hr) | Reference velocity* ( km s$^{-1}$) | 1-$\sigma$ level noise (mJy beam$^{-1}$) | Synthesized beam† (mas) | Number of detected features |
|---|---|---|---|---|---|---|
| r05083a ... | March 24 | 7.5 | −3.6 | 31 | 7.5×3.4, −79° | 20 |
| r05117b .. | April 27 | 9.5 | −3.4 | 21 | 7.4×3.4, −70° | 18 |
| r05148a ... | May 28 | 9.6‡ | −3.4 | 19 | 7.2×3.3, −64° | 10 |

* Velocity channel used for the phase reference in data reduction.
† The synthesized beam made in natural weight; major and minor axis lengths and a position angle.
‡ Valid operation for 6 hr in the Nobeyama 45 m telescope.

**Table 2.** Parameters of the detected $H_2O$ maser features in WX Psc.

| Date | $V_{\rm LSR}$ * (km s$^{-1}$) | RA offset† (mas) | Dec offset† (mas) | $I_{\rm peak}$‡ (Jy beam$^{-1}$) | $\Delta V$§ (km s$^{-1}$) | F# ‖ |
|---|---|---|---|---|---|---|
| 2005 March 24 | 25.65 | −33.731±0.465 | 46.530±0.140 | 0.78 | 0.84 | 13 |
| | 22.98 | −0.560±1.629 | 50.010±2.187 | 1.91 | 0.84 | |
| | 22.96 | −12.490±0.042 | 62.423±0.330 | 5.50 | 1.05 | 12 |
| | 22.56 | −12.080±0.033 | 69.470±1.080 | 3.32 | 0.84 | |
| | 22.38 | −3.677±0.241 | 54.635±0.203 | 3.75 | 0.63 | 11 |
| | 21.70 | 3.578±0.516 | 62.515±1.200 | 3.77 | 1.05 | 10 |
| | 20.66 | −7.290±0.112 | 86.200±0.095 | 0.66 | 0.42 | |
| | −1.04 | 0.080±0.448 | 61.870±0.242 | 0.49 | 0.42 | |
| | −1.25 | −0.420±0.286 | 70.340±0.133 | 0.40 | 0.42 | 9 |
| | −1.69 | −1.170±0.290 | 61.106±0.503 | 0.80 | 0.84 | 8 |
| | −1.88 | 10.220±0.199 | 11.910±0.356 | 0.86 | 0.42 | |
| | −2.31 | 10.800±0.633 | 1.800±1.225 | 1.30 | 0.84 | 7 |
| | −3.36 | 1.440±0.433 | −7.900±0.332 | 2.10 | 0.63 | 5 |
| | −3.36 | −1.740±0.052 | 8.470±0.353 | 2.03 | 0.42 | 6 |
| | −3.60 | 0.302±1.125 | −0.140±1.265 | 18.75 | 1.90 | 4 |
| | −4.20 | −27.030±1.858 | 37.980±0.413 | 3.21 | 0.84 | |
| | −4.83 | −23.890±0.310 | 38.640±0.137 | 1.33 | 0.42 | |
| | −4.99 | −11.920±0.650 | 36.148±0.057 | 1.66 | 1.05 | 3 |
| | −5.04 | −22.990±0.102 | 29.880±0.174 | 1.06 | 0.42 | 2 |
| | −5.89 | −14.667±0.252 | 43.984±0.432 | 0.52 | 0.63 | 1 |
| 2005 April 27 | 25.67 | −33.978±0.293 | 46.402±0.078 | 0.56 | 0.63 | 13 |
| | 25.42 | −33.440±3.416 | 54.870±0.173 | 0.24 | 2.11 | |
| | 23.73 | 2.080±0.100 | 55.370±0.073 | 0.57 | 0.42 | |
| | 23.03 | −12.493±0.051 | 62.776±0.327 | 4.84 | 1.05 | 12 |
| | 22.47 | −3.260±0.851 | 54.560±0.368 | 2.75 | 0.63 | 11 |
| | 21.79 | 3.456±1.054 | 62.892±0.813 | 4.00 | 1.05 | 10 |
| | 21.20 | 6.800±0.839 | 54.140±0.179 | 1.89 | 0.42 | |
| | −1.55 | −0.610±0.902 | 70.180±0.448 | 0.48 | 0.84 | 9 |
| | −1.97 | −2.110±1.335 | 61.060±0.643 | 0.88 | 1.26 | 8 |
| | −2.17 | 10.362±0.445 | 2.612±0.741 | 1.57 | 1.05 | 7 |
| | −3.40 | −0.770±0.907 | 8.509±0.158 | 2.06 | 0.63 | 6 |
| | −3.44 | 1.140±0.570 | −8.060±0.512 | 2.23 | 0.63 | 5 |
| | −3.67 | 0.355±1.073 | −0.202±1.217 | 15.33 | 1.68 | 4 |
| | −4.29 | −27.510±0.327 | 46.560±0.079 | 2.16 | 0.42 | |
| | −5.07 | −12.273±0.079 | 36.346±0.061 | 1.34 | 0.63 | 3 |
| | −5.10 | −22.972±0.097 | 29.912±0.227 | 1.03 | 0.63 | 2 |
| | −5.55 | −15.260±0.480 | 53.080±0.158 | 0.42 | 0.42 | |
| | −5.94 | −14.826±0.365 | 44.175±0.332 | 0.35 | 0.63 | 1 |
| 2005 May 28 | 25.69 | −34.066±0.284 | 46.532±0.163 | 0.37 | 0.63 | 13 |
| | 23.18 | −12.710±0.481 | 63.307±0.489 | 4.09 | 0.84 | 12 |
| | 21.89 | 3.324±0.752 | 62.927±0.758 | 3.70 | 0.84 | 10 |
| | −1.32 | 0.020±0.472 | 70.505±0.191 | 0.58 | 0.63 | 9 |
| | −2.13 | 10.290±0.371 | 2.900±0.617 | 1.63 | 0.42 | 7 |
| | −3.39 | 0.370±0.236 | −8.330±0.388 | 2.33 | 0.42 | 5 |
| | −3.39 | −0.370±0.770 | 8.770±0.240 | 1.93 | 0.42 | 6 |
| | −3.72 | 0.385±0.488 | −0.293±0.677 | 12.72 | 1.26 | 4 |
| | −5.06 | −12.125±0.207 | 36.300±0.170 | 1.21 | 0.63 | |
| | −5.92 | −14.900±0.281 | 44.410±0.220 | 0.29 | 0.42 | 1 |

* A local-standard-of-rest velocity at the intensity peak.
† Position offset with respect to the maser spot in the phase-reference velocity channel (see the main text).
‡ A peak intensity of the feature.
§ A full velocity width with maser emission. The minimum is equal to a velocity spacing of a spectral channel (0.21 km s$^{-1}$).
‖ Maser feature listed in table 3. The feature is designated as WX Psc:I2007 *N*, where *N* is the ordinal source number given in this column (I2007 stands for sources found by Inomata et al. and listed in 2007).

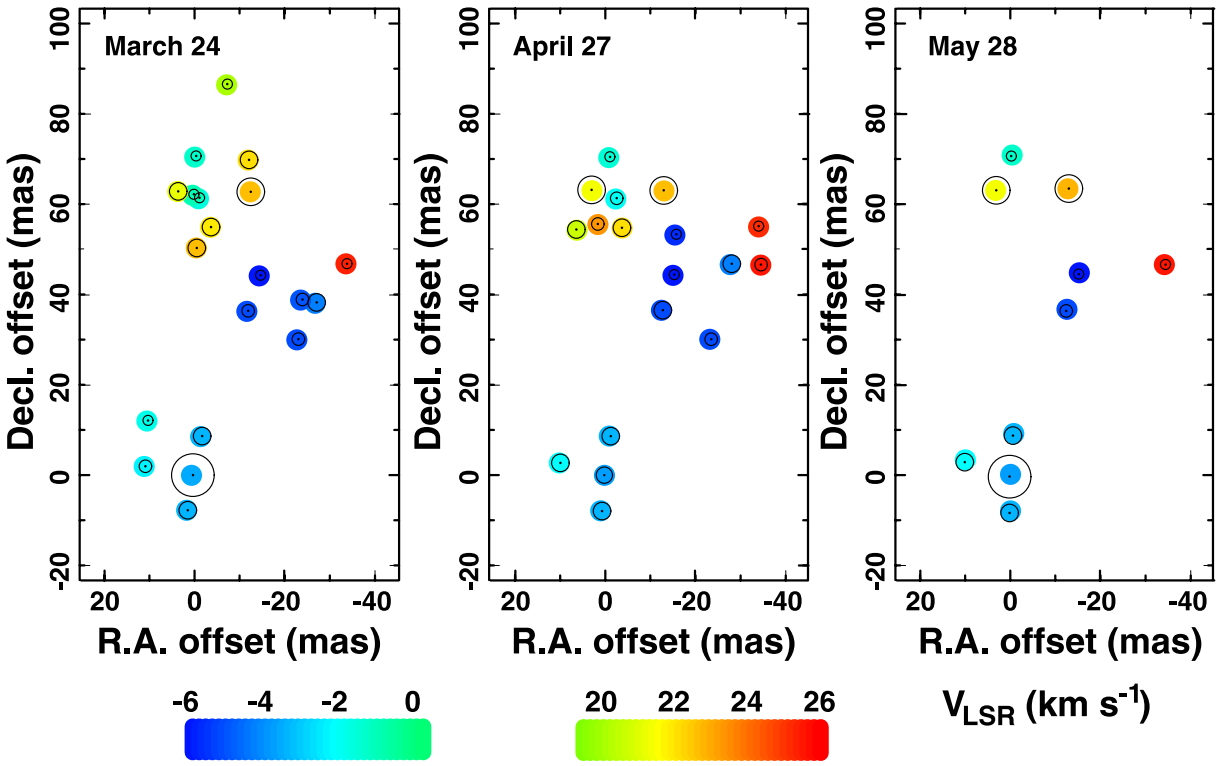


**Fig. 2.** Spatial distributions of $H_2O$ maser features in WX Psc at the three epochs. The size of a black circle around the feature indicates the logarithmically scaled peak intensity of the feature.

**Table 3.** Relative proper motions of $H_2O$ maser features in WX Psc.

| Maser feature* (WX Psc: I2007) | Offset† (mas) | | Proper motion† (mas yr$^{-1}$) | | | | Radial motion‡ (km s$^{-1}$) | | Peak intensity at 3 epochs (Jy beam$^{-1}$) | | |
|---|---|---|---|---|---|---|---|---|---|---|---|
| | RA | Dec | $\mu_x$ | $\sigma\mu_x$ | $\mu_y$ | $\sigma\mu_y$ | $V_z$ | $\Delta V_z$§ | Epoch 1 | Epoch 2 | Epoch 3 |
| 1 ..... | −14.97 | 44.12 | −1.77 | 2.09 | 3.33 | 2.56 | −5.89 | 0.56 | 0.52 | 0.35 | 0.29 |
| 2 ..... | −23.29 | 30.02 | −0.37 | 1.47 | 0.98 | 3.00 | −5.04 | 0.52 | 1.06 | 1.03 | ... |
| 3 ..... | −12.22 | 36.29 | 0.62 | 2.41 | 2.29 | 0.72 | −4.99 | 0.77 | 1.66 | 1.34 | 1.21 |
| 4 ..... | 0.00 | 0.00 | 0.00 | 6.47 | 0.00 | 7.71 | −3.60 | 1.61 | 18.75 | 15.33 | 12.72 |
| 5 ..... | 1.14 | −7.76 | −6.63 | 2.69 | −1.52 | 2.82 | −3.36 | 0.56 | 2.10 | 2.23 | 2.33 |
| 6 ..... | −2.04 | 8.61 | 7.56 | 3.91 | 2.83 | 2.30 | −3.36 | 0.49 | 2.03 | 2.06 | 1.93 |
| 7 ..... | 10.50 | 1.94 | −2.95 | 3.92 | 6.37 | 7.08 | −2.31 | 0.77 | 1.30 | 1.57 | 1.63 |
| 8 ..... | −1.47 | 61.25 | −10.40 | 14.31 | 0.17 | 8.55 | −1.69 | 1.05 | 0.80 | 0.88 | ... |
| 9 ..... | −0.72 | 70.48 | 1.77 | 3.03 | 1.69 | 1.29 | −1.25 | 0.63 | 0.40 | 0.48 | 0.58 |
| 10 ..... | 3.28 | 62.65 | −1.87 | 5.00 | 2.89 | 7.64 | 21.70 | 0.98 | 3.77 | 4.00 | 3.70 |
| 11 ..... | −3.98 | 54.77 | 3.81 | 9.26 | −0.14 | 4.40 | 22.38 | 0.63 | 3.75 | 2.75 | ... |
| 12 ..... | −12.79 | 62.56 | −0.64 | 0.68 | 5.47 | 3.14 | 22.96 | 0.98 | 5.50 | 4.84 | 4.09 |
| 13 ..... | −34.03 | 46.67 | −2.16 | 2.91 | 0.64 | 1.18 | 25.65 | 0.70 | 0.78 | 0.56 | 0.37 |

* Water-maser feature detected toward WX Psc. The feature is designated as WX Psc:I2007 *N*, where *N* is the ordinal source number given in this column (I2007 stands for sources found by Inomata et al. and listed in 2007).
† Relative value with respect to the motion of the position-reference maser feature: WX Psc:I2007 *4*.
‡ Relative value with respect to the local-standard-of-rest.
§ Mean full velocity width of a maser feature at half intensity.

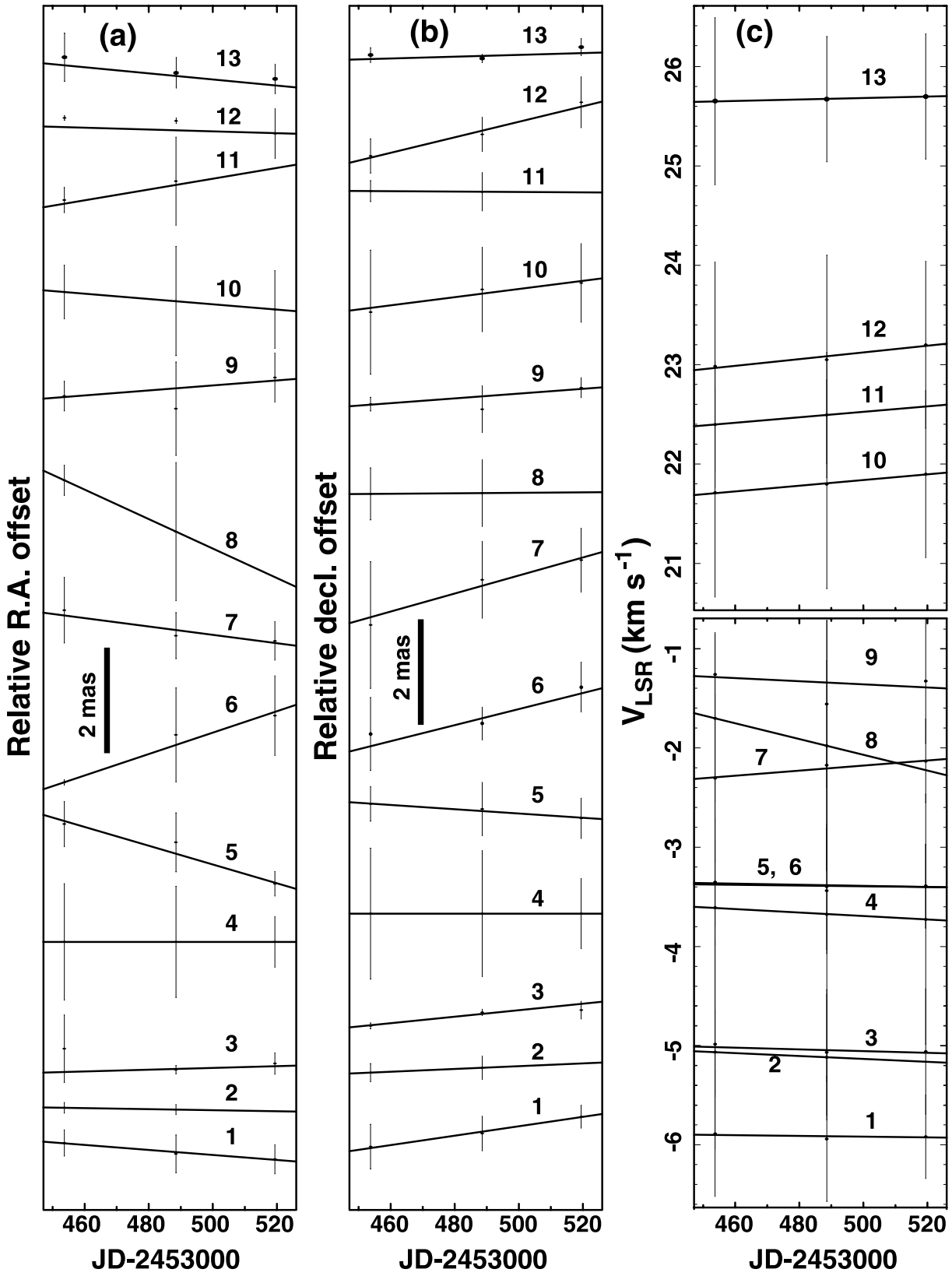


**Fig. 3.** Observed relative proper motions (panels a and b) and Doppler velocity variations (panel c) of $H_2O$ maser features in WX Psc. A number shown alongside each maser motion is the assigned one after the designated name form "WX Psc: I2007" (see table 3). A solid line in the position or Doppler velocity plot indicates a least-squares-fitted line assuming a constant velocity motion in the proper motion or a constant Doppler velocity drift.

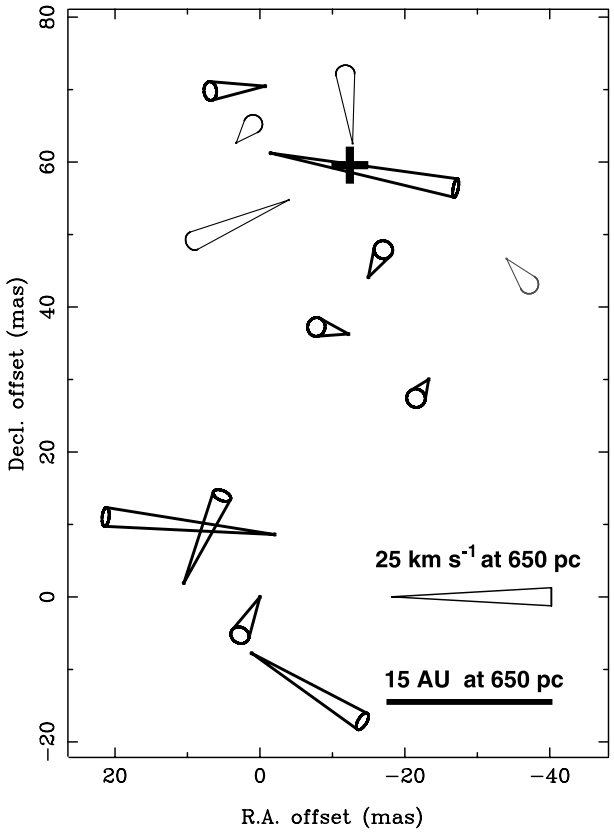


**Fig. 4.** Proper motions of the $H_2O$ maser features. The origin of a cone indicates the maser feature position, and the direction and length of the cone indicate the three-dimensional velocity vector of the proper motion. Thick and thin cones indicate those blueshifted and redshifted with respect to the systemic velocity, respectively. The mean velocity vector of the maser cluster, $(\langle \Delta V_x \rangle, \langle \Delta V_y \rangle) = (-2.8, 5.3)$[ km s$^{-1}$], is subtracted from the calculated velocity vector. A plus symbol indicates the location of the dynamical center of the modeled radially expanding flow.

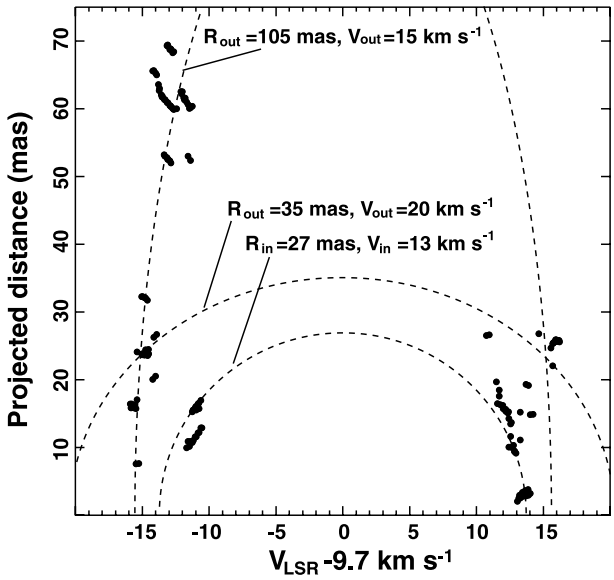


**Fig. 5.** Projected distance–radial-velocity diagram of the $H_2O$ maser spots in WX Psc. The modeled inner and outer boundaries of a spherically expanding thick shell are indicated with dashed lines. Another thin shell including the southern maser components and the most blueshifted components is also indicated.

**Table 4.** Diagonalization analysis.*

| Eigenvalue $[(\mathrm{km\,s^{-1}})^2]$ | Eigenvector Inclination | Position angle |
|---|---|---|
| Velocity variance-covariance matrix | | |
| 278± 48 | −6°± 10° | 96°±13° |
| 172± 5 | 78°± 11° | 64°±70° |
| 95± 14 | −2°± 10° | 6°±10° |
| Spatial variance-covariance matrix (mas$^2$) | | |
| 823 | ... | −9° |
| 117 | ... | 81° |

* Diagonalization analysis of the variance-covariance matrix of the velocity and position vectors of the WX Psc $H_2O$ masers.

a radius of $R_{\rm out}$ ∼40 mas (mentioned above), an expansion velocity of $V_{\rm out}$ ≃15 km s$^{-1}$ is obtained. However, this model does not encompass the possibility that the circumstellar envelope is radially accelerated in the $H_2O$ maser regions, as is commonly found in Mira variables. On the contrary, the southern group of features exhibits a radial alignment of maser spots from the diagram origin, indicating radial acceleration in the region. Therefore, it is expected that the southern maser group is located at a larger radius, and that the $H_2O$ masers in WX Psc are grouped into two types: one associated with a spherically expanding envelope and another with a flow in the SSE direction.

In order to undertake an objective analysis, we also applied the variance-covariance matrix (VCM) diagonalization procedure (Bloemhof 1993, 2000) for the observed maser proper motion vectors and locations. The velocity VCM consists of elements calculated from velocity dispersions, $\sigma_{ij}$, as follows:

$$\sigma_{ij} = \frac{1}{N-1}\sum_{n=1}^{N}(v_{i,n} - \overline{v}_i)(v_{j,n} - \overline{v}_j), \qquad (2)$$

where $i$ and $j$ denote three orthogonal space axes (e.g., RA, Dec, and radial coordinate $z$), $n$ the $n$-th maser motion in a collection totaling $N$, and the bar averaging over the maser motions. They are diagonalized to obtain eigenvalues and their corresponding eigenvectors. In order to estimate the most reliable eigenvalues, corresponding eigenvectors, and their uncertainty, we performed a Monte Carlo simulation, in which the individual maser motions were randomly varied from the observed values within the measurement errors (see Imai et al. 2006). Table 4 gives the results. Note that the uncertainties of the eigenvector inclinations may be larger than those given in table 4, because of some uncertainty of the distance to WX Psc. In the same way as for the velocity VCM, the spatial VCM is also diagonalized; the results are also shown in table 4.

The eigenvector giving the largest eigenvalue indicates the kinematical major axis of the outflow. However, if a difference between the largest and second-largest eigenvalues

is smaller than that between the second-largest and smallest ones, then the maser motions are dispersed in the plane containing the eigenvectors corresponding to the largest and second-largest eigenvalues, or in the plane perpendicular to the eigenvector corresponding to the smallest eigenvalue. This implies that the flow in WX Psc is equatorially expanding with the latter eigenvector pointed in the north–south orientation, as is the kinematical axis. This axis is roughly coincident with the morphological major axis of the bispectrum speckle interferometry near-infrared $J$-band image, which has a symmetry axis with a position angle of $PA = -28°$ (H01). It is pole-on, and roughly consistent with that predicted by a radiative transfer simulation model proposed by V04 (an inclination with respect to the line of sight, $i = 25°$). Note that the line-of-sight velocity gradient of the masers, including the southern feature group, is inverted from that in the model, in which the blueshifted maser components should be located in the NNW direction rather than in the SSE direction if the flow is collimated into this kinematical axis.

## 4. Discussion

The present VLBI observations of $H_2O$ masers in WX Psc offer us detailed kinematic information on the circumstellar envelope of WX Psc and an opportunity to examine the model proposed by V04 for the envelope. The observed $H_2O$ maser spectrum exhibits clear double peaks, quite similar to those found in 1612 MHz OH maser emission of Mira variables and OH/IR stars, which traces the outer layer of the circumstellar envelope spherically expanding in a constant velocity (20–30 km s$^{-1}$). In these stars, however, $H_2O$ maser spectra usually exhibit triple or multiple peaks with a velocity range correlated with the mass-loss rate or evolutionary status of the accompanying star (Takaba et al. 1994). These may be understood by the fact that the $H_2O$ maser emission in these stars is associated with a larger range of orders of magnitude in the envelope radius (10–100 AU) than 1612 MHz OH maser emission ($\sim$1000 AU) is, and that only $H_2O$ maser regions exhibit radial acceleration (e.g., Elitzur 1992; Bains et al. 2003). The exceptions for the $H_2O$ maser spectrum are the spectra found in the "water fountain" sources in which the spectrum exhibits double peaks separated by as much as 100 km s$^{-1}$ (e.g., Imai et al. 2002). However, as described above, the spatiokinematics of the WX Psc flow is much less collimated than those in the water fountain sources. A spherically symmetric expanding flow is also expected to exhibit a similar less-collimated flow, but the line-of-sight velocity gradient in the WX Psc $H_2O$ masers, including the southern maser feature group, is different from that expected from such a symmetric or bipolar outflow. Therefore, we need to analyze the $H_2O$ spatiokinematics in more detail without the assumption of a spherically uniform flow in the envelope. It should be taken into account that strong maser amplification occurs through a line of sight that is geometrically thick and coherent in velocity. Because the $H_2O$ maser spectrum (see figure 1) clearly shows double peaks, which are separated by $\sim$25 km s$^{-1}$ while each has a velocity width of only $\sim$5 km s$^{-1}$, it is expected that the spatiokinematical structure is so simple that the maser excitation regions are limited in space and velocity.

As one of the suitable spatiokinematical models, we here demonstrate the model proposed by V04. V04 performed 2D radiative transfer calculations of a two-component model for the WX Psc envelope: a spherically symmetric wind and biconical cocoons driven by a bipolar jet. These components have different mass-loss rates and density profiles, each as a function of the radius. V04 suggests that the asymmetric morphology in the $J$-band image (H01) indicates the existence of a bipolar outflow with a dynamical age shorter than 200 yr. On the basis of the expansion velocity, we reestimated the dynamical age of the bipolar outflow to be $\sim$300 yr. As mentioned above, the observed flow seems to be equatorially expanding with a symmetric axis parallel to the V04 model. Alternatively, it still remains a possibility that a collimated jet exists, and that its major axis is pointed to a different inclination from this model. For example, the southern maser feature group traces the approaching side of the collimated jet that is precessing. We discuss these two possibilities below.

*Model 1 : A biconically expanding outflow*

In order to explain both the radial-velocity distribution of the $H_2O$ masers (figure 2) and the fan-shaped structure seen in the $J$-band image (H01) consistently, we suggest a biconically expanding flow model, as adopted by Imai et al. (2005), in which $H_2O$ maser emission is excited in a circumstellar envelope surrounding a bipolar jet in a density cavity. In the model we consider a volume density profile determined by mass conservation in the spatiokinematical structure of flow. We calculated the maser gains along all lines of sight, which are proportional to the gas density and the path length of the radial-velocity coherence (within 1 km s$^{-1}$) under saturated maser conditions. The assumption of saturated masers simplifies the calculations, and is reasonable when taking into account the temporally stable spectrum of masers. Radiation pressure on circumstellar dust accelerates the flow in the $H_2O$ maser region, giving the flow velocity, $v$, as a function of the radius (Elitzur 1992; Elitzur et al. 2003),

$$v^2 = v_\infty^2(1 - r_0/r), \tag{3}$$

where $r_0$ is the inner radius of the dust envelope or the base of the flow, and $v_\infty$ the terminal velocity at the outer edge of the envelope. This functional form is consistent with velocity fields actually observed around some circumstellar envelopes (e.g., Bains et al. 2003). A systemic velocity, $V_{\rm LSR}$=10 km s$^{-1}$, and a terminal velocity, $v_\infty = 20$ km s$^{-1}$, are adopted (Baud 1981; Loup et al. 1993). An inclination with respect to the line of sight, $i = 25°$, a position angle, $PA = -30°$, and an inner radius of the flow, $r_0 = 35$ mas, are also adopted (V04). Figure 6 shows the best-fit biconical flow model. A cavity that corresponds to a jet consisting of a lower density gas is needed to have a wide half opening angle from the flow axis ($\theta_{\rm cone} \geq 35°$) and to create the observed line-of-sight velocity gradient of $H_2O$ masers, in which the redshifted and blueshifted maser features are located in the NNW and SSE directions, respectively. In this configuration, the most blueshifted and redshifted maser components are apparently overlapped at the stellar location. Note that each of the blueshifted and redshifted feature distributions extends perpendicularly to the jet major axis (NNW–SSE orientation).

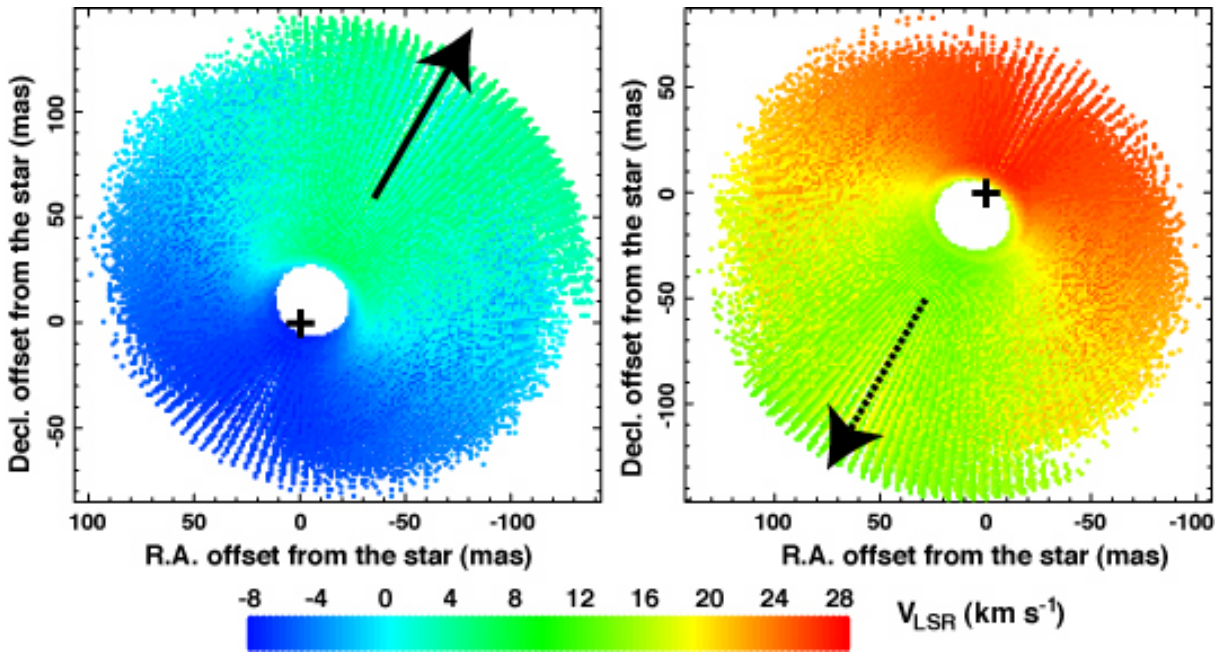


**Fig. 6.** Biconically expanding flow model fit to the spatiokinematical structure of $H_2O$ masers around WX Psc. A position angle of $-30°$ and an inclination of 25° with respect to the line of sight are adopted for the flow axis. Inner and outer half opening angles of the bicone $\theta_{\rm cone}$ =35° and 60° are adopted, respectively. At each location, a radial velocity having the largest gain of maser amplification is indicated by a colored filled circle. The gains at the filled circles are larger than 5% of the maximum gain in the sky field. A plus indicates the location of the central star. *Left panel*: A modeled cone opening toward the observer. A solid-line arrow indicates the approaching flow direction. *Right panel*: Same as the left panel but opening against the observer. A dashed-line arrow indicates the receding-flow direction.

If an equatorial flow is predominant ($\theta_{\rm cone} \sim 90°$), both components will be completely blended, because the receding and approaching sides of the flow roughly obtain an equal maser gain. The observed distribution is, however, mildly split, and the flow may be expanding biconically rather than equatorially ($\theta_{\rm cone} \leq 60°$). A wide spread of the southern blueshifted maser components (up to 60 mas) suggests that they are located at a large radius of the flow ($r \geq$150 mas), in which the acceleration of the flow is reduced. The absence of redshifted components $\sim$ 50 mas north of the star is explained by a lower maser gain and broadening over the angular resolution of the interferometer due to the foreground approaching envelope, as proposed by Takaba et al. (1994).

On the other hand, the bipolar flow modeled by V04 has an opening angle of $\theta_{\rm cone} = 30°$, which is smaller than the inner opening angle of the biconical $H_2O$ maser flow ($\theta_{\rm cone} \geq 35°$), implying that the bipolar and biconical flows are spatially well shared. The density profiles in the bipolar and biconical flows are proportional to $r^{-0.5}$ and $r^{-2}$, respectively, in the V04 model. In these profiles, the latter has a higher gas density than the former in the region close to the central star or the flow base. Thus, this model suggests that the $H_2O$ masers are associated with a wide-angled, biconically expanding flow with a higher gas density, rather than a collimated bipolar outflow. This model can cover the whole velocity range of $H_2O$ maser emission ($-8 \leq V_{\rm LSR} \leq 28$ km s$^{-1}$). However, the maser amplification around the stellar velocity ($V_{\rm LSR}\sim$10 km s$^{-1}$) is smaller than that around the flow velocity ($V_{\rm LSR}\sim -5$, 25 km s$^{-1}$), leading to the formation of a double-peaked maser spectrum.

*Model 2 : A precessing collimated bipolar outflow*

Suppose that the $H_2O$ masers are associated with a collimated outflow, itself undergoing precession. The blueshifted maser components $\sim$60 mas away from the central star (see figure 5) can be associated with such a collimated outflow. Adopting an inclination of the flow of $i = 25°$, for instance, and a distance to WX Psc of $D = 650$ pc, these components are located at $\sim$90 AU from the star, and the dynamical time scale of the $H_2O$ maser flow is obtained to be $\sim$20 yr. The radius of maser emission is still similar to that typically found in AGB stars (e.g., Bowers & Johnston 1994). The dynamical time scale is an order of magnitude smaller than that of the flow seen in the $J$-band image on the larger scale ($\leq$200 yr in V04 but $\sim$ 300 yr in the present work). This may imply that the outflow axis pointed to the NNW 200–300 yr ago, although recently within 20 yr it points to the SSE. However, it is difficult to create a clear radial velocity gradient if the outflow axis direction has continuously changed and the mass loss from the star has been stable for 200 yr. It is possible that the $H_2O$ masers have been excited only in the region where we are detecting them because the outer region of the flow still has too small a gas density to excite the masers.

We note here the angular distributions of SiO masers around WX Psc with a radius of $\sim$10 mas revealed by Soria-Ruiz et al. (2004). They are qualitatively similar to those typically found in Mira variables or AGB stars, and roughly exhibit a circular ring. It is quite different from that found in W43A, which has a highly collimated jet (Imai et al. 2005). The SiO masers in W43A exhibit a clear velocity gradient with the same trend as that found in the high-velocity $H_2O$ masers, and have

an expansion velocity of $\sim$16 km s$^{-1}$, which is much larger than the velocity dispersion found in the WX Psc SiO masers ($\leq$3 km s$^{-1}$). Thus no support for the existence of a highly collimated jet is found in WX Psc. To examine the existence of such a collimated jet, we need more detailed information on the maser spatiokinematics by increasing the number of detected maser features and the measured proper motions. This may be possible with high-precision astrometry achieved with the VERA, because it provides us absolute positions of maser features through long-term monitoring observations in a common coordinate system after subtracting an annual parallax and a systematic secular motion. After these procedures, point symmetric maser spatiokinematical structure, if discovered, may give strong evidence for such a collimated flow.

In both models flow acceleration should be taken into account to form high velocity jets seen in water fountain sources (e.g., W43A). Expansion velocities of both the WX Psc envelope and jet are only $\sim$20 km s$^{-1}$ at present. Boboltz and Marvel(2005) found the acceleration rate in the radial velocity to be 0.68 km s$^{-1}$ yr$^{-1}$ in one of the water fountain sources, OH 12.8$-$0.9. With the same acceleration rate, the WX Psc jet also may be accelerated up to 100 km s$^{-1}$ with an estimated duration of the water fountain sources ($\leq$100 yr, e.g., Imai et al. 2004).

## 5. Summary

We have demonstrated the existence of a collimated bipolar flow in the AGB star WX Psc with VLBI observations of the $H_2O$ masers. WX Psc is believed to show the sign of a collimated jet launch, which is suggested by a fan-shaped morphology found in near-infrared emission. We reestimated the expansion velocity of the circumstellar envelope and its dynamical age to be $\sim$16 km s$^{-1}$ and $\sim$300 yr, respectively, on the basis of the maser spatiokinematical structure. The $H_2O$ masers themselves may be associated with the circumstellar envelope that is biconically expanding with a wider opening angle from the flow axis. However, the masers strongly support the existence of a collimated bipolar outflow in the cavity surrounded by the $H_2O$ maser envelope. This configuration may occur at the earliest phase of stellar jet formation, in which the gas density of the circumstellar envelope with $H_2O$ maser emission is higher than that of the jet, itself, near the driving star. It is expected that at the later stage, the $H_2O$ maser locations should be switched from the AGB envelopes to the jets, such as water fountain sources, like W43A. The stellar jets in the water fountain sources have short dynamical ages ($\leq$100 yr, e.g., Imai et al. 2004), which may also be comparable to the time scale of the location switching of $H_2O$ masers.

We acknowledge all staff members and students who have helped in array operation and in data correlation of the JVN/VERA. We also thank to Dr. Shuji Deguchi, a referee, and Phil Diamond for a careful reading of the manuscript and providing critical suggestions. T.O./H.I. and H. I. have been financially supported by Grants-in-Aid for Scientific Research from Japan Society for the Promotion Science (17340055 and 18740109).

## References

Bains, I., Cohen, R. J., Louridas, A., Richards, A. M. S., Rosa-González, D., & Yates, J. A. 2003, MNRAS, 342, 8
Baud, B. 1981, ApJ, 250, L79
Blackman, E. G., Frank, A., Markiel, J. A., Thomas, J. H., & van Horn, H. M. 2001, Nature, 409, 485
Blair, G. N., & Dickinson, D. F. 1977, ApJS, 215, 552
Bloemhof, E. E. 1993, ApJ, 406, L75
Bloemhof, E. E. 2000, ApJ, 533, 893
Boboltz, D. A., & Marvel, K. B. 2005, ApJ, 627, L45
Bowers, P. F., & Johnston, K. J. 1994, ApJS, 92, 189
Bowers, P. F., Johnston, K. J., & Spencer, J. H. 1983, ApJ, 274, 733
Cernicharo, J., Alcolea, J., Baudry, A., & González-Alfonso, E. 1997, A&A, 319, 607
Comoretto, G., et al. 1990, A&AS, 84, 179
Desmurs, J. F., Bujarrabal, V., Colomer, F., & Alcolea, J. 2000, A&A, 360, 189
Diamond, P. 1989, in Very Long Baseline Interferometry, Techniques and Applications, ed. M. Felli & R. E. Spencer (Dordrecht: Kluwer Academic Publishers), 231
Diamond, P. J. 1995, ASP Conf. Ser., 82, 227
Diamond, P. J., Kemball, A. J., Junor, W., Zensus, A., Benson, J., & Dhawan, V. 1994, ApJ, 430, L61
Dickinson, D. F., Reid, M. J., Morris, M., & Redman, R. 1978, ApJ, 220, L113
Dyck, H. M., Lockwood, G. W., & Capps, R. W. 1974, ApJ, 189, 89
Elitzur, M. 1992, Astronomical Masers (Dordrecht: Kluwer Academic Publishers)
Elitzur, M., Ivezić, Ž., & Vinković, D. 2003, in Mass-Losing Pulsating Stars and their Circumstellar Matter, Observations and Theory, ed. Y. Nakada, M. Honma, & M. Seki (Dordrecht: Kluwer Academic Publishers), 265
Greenhill, L. J., Colomer, F., Moran, J. M., Backer, D. C., Danchi, W. C., & Bester, M. 1995, ApJ, 449, 365
Hofmann, K.-H., Balega, Y., Blöcker, T., & Weigelt, G. 2001, A&A, 379, 529 (H01)
Hyland, A. R., Becklin, E. E., Frogel, J. A., & Neugebauer, G. 1972, A&A, 16, 204
Imai, H., Kameya, O., Sasao, T., Miyoshi, M., Deguchi, S., Horiuchi, S., & Asaki, Y. 2000, ApJ, 538, 751
Imai, H., Morris, M., Sahai, R., Hachisuka, K., & Azzollini, J. R. F. 2004, A&A, 420, 265
Imai, H., Nakashima, J., Diamond, P. J., Miyazaki, A., & Deguchi, S. 2005, ApJ, 622, L125
Imai, H., Obara, K., Diamond, P. J., Omodaka, T., & Sasao, T. 2002, Nature, 417, 829
Imai, H., Omodaka, T., Hirota, T., Umemoto, T., Sorai, K., & Kondo, T. 2006, PASJ, 58, 883
Kwok, S., Purton, C. R., & FitzGerald, P. M. 1978, ApJ, 219, L125
Le Bertre, T. 1993, A&AS, 97, 729
Lockwood, G. W. 1985, ApJS, 58, 167
Loup, C., Forveille, T., Omont, A., & Paul, J. F. 1993, A&AS, 99, 291
Miyoshi, M., Matsumoto, K., Kameno, S., Takaba, H., & Iwata, T. 1994, Nature, 371, 395
Morris, M. R., Sahai, R., & Claussen, M. 2003, Rev. Mex. Astron. Astrofis. (Ser. Conf.), 15, 20

Olnon, F. M., Winnberg, A., Matthews, H. E., & Schultz, G. V. 1980, A&AS, 42, 119
Soria-Ruiz, R., Alcolea, J., Colomer, F., Bujarrabal, V., Desmurs, J.-F., Marvel, K. B., & Diamond, P. J. 2004, A&A, 426, 131
Soria-Ruiz, R., Colomer, F., Alcolea, J., Bujarrabal, V., Desmurs, J.-F., & Marvel, K.B. 2005, A&A, 432, L39
Takaba, H., Ukita, N., Miyaji, T., & Miyoshi, M. 1994, PASJ, 46, 629
te Lintel Hekkert, P., Versteege-Hensel, H. A., Habing, H. J., & Wiertz, M. 1989, A&AS, 78, 399
van Langevelde, H. J., van der Heiden, R., & van Schooneveld, C. 1990, A&A, 239, 193
Vinković, D., Blöcker, T., Hofmann, K.-H., Elitzur, M., & Weigelt, G. 2004, MNRAS, 352, 852 (V04)
Vlemmings, W. H. T., Diamond, P. J., & Imai, H. 2006, Nature, 440, 58
Whitelock, P., Menzies J., Feast, M., Marang, F., Carter, B., Roberts, G., Catchpole, R., & Chapman, J. 1994, MNRAS, 267, 711
Wilkinson, P. N. 1989, in Very Long Baseline Interferometry, Techniques and Applications, ed. M. Felli & R. E. Spencer (Dordrecht: Kluwer Academic Publishers), 69
Wilson, W. J., Barrett, A. H., & Moran, J. M. 1970, ApJ, 160, 545